Biophysical Journal, Volume 99

Supporting Material

Optimizing Methods to Recover Absolute FRET Efficiency from Immobilized Single Molecules

James J. McCann, Ucheor B. Choi, Liqiang Zheng, Keith Weninger, and Mark E. Bowen

Supporting Materials

Optimizing Methods to Recover Absolute FRET Efficiency from Immobilized Single Molecules

James J. McCann, Ucheor B. Choi, Liqiang Zheng, Keith Weninger and Mark E. Bowen

Supporting Methods

Fluorescence Microscopy

Quartz slides were cleaned by sequential sonication in detergent, acetone, ethanol and potassium hydroxide. Slides were coated with biotinylated Bovine Serum Albumin (BSA) (Sigma-Aldrich, St. Louis, MO) followed by streptavidin (Invitrogen, Carlsbad, CA). Labeled samples were diluted to a sufficiently low concentration so as to capture 100-200 molecules per field of view with 5 minutes incubation (typically pM). Donor excitation used a circularly polarized, 20 mW diode-pumped 532 nm continuous wave laser. Acceptor excitation used a 25 mW laser diode at 633 nm (Newport Corporation, Irvine, CA). Mechanical shutters (Uniblitz, Rochester, NY) were used to alternate the laser excitation. Donor and acceptor images were split using an Optosplit Image Splitter (Cairn Research Ltd, Faversham, UK). Images were recorded with an electron-multiplied CCD camera (either iXon (Andor Technologies, Belfast, UK) or a Cascade 512B (Roper Scientific, Tucson, AZ)).

Data Analysis

Data collection and processing were performed as described previously (1, 2). Single acceptor molecules were identified using an average image generated from 10 frames acquired with100 msec resolution during 633 nm illumination. Single molecules were selected as pixels with intensity values 7 fold higher than the standard deviation of the background fluorescence that are also the local maxima within a 3 x 3 pixel window and separated by 5 or more pixels from any neighboring maxima. Donor and acceptor images are mapped on to one another using a normalized 2-D cross-correlation of a separately collected image of immobilized fluorescent beads with a broadband emission spectrum such that each bead has emission in both channels. This cross-correlation mapping provides the initial offset values for the expected location of the donor dye based on the location of the acceptor dye found as described above. The expected donor location provided the starting point for an empirical search for the donor dye, as was done with the acceptor, by identifying the local maxima within a 3 x 3 pixel about the expected position. The average selected single molecule appears as a centered, 2D circular Gaussian peak. The value for the single molecule intensity is taken as the sum of the four most intense pixels within the 3 by 3 matrix centered on the maxima. The initial location of the empirically-found

peak is used to calculate intensity at each frame of the movie. Local background fluorescence was determined from the median pixel value within a 32 x 32 pixel window. Local background was calculated separately for each laser phase and subtracted from each frame of the movie. Omitting background subtraction did not significantly alter the values for $\gamma^{Photobleach}$ (data not shown) because the background intensity is similar for both the donor and acceptor channels. According to Eqn. 5, $\gamma^{Photobleach}$ is calculated from a ratio of acceptor and donor intensities so the ratio of the background intensities is one. In addition, for the Andor camera the background intensity at empty pixels is typically less than 10% of the emission intensity from pixels containing a single molecule. Leakage of donor excitation through the optical filters into the acceptor channel was measured using singly-labeled proteins. The value of γ was calculated using a 20 point average intensity of both channels and Eq. 6. We found that γ did not correlate with the width of the raw E_{PR} distribution or the magnitude of the intensity change during the photobleaching event used to calculate γ (data not shown). Correcting entire data sets for γ (i.e. "universal" or "global" γ correction) can be accomplished by taking the mean value of γ obtained from the subset of acceptor bleaching events and adjusting the FRET efficiency of all hand-selected single pair FRET events using

$$FRET = \left(\frac{E_{PR}}{(E_{PR} + \gamma - \gamma E_{PR})}\right) \quad \text{(S1)}$$

where E_{PR} is the raw FRET efficiency corrected for donor leakage into the acceptor channel. This equation is useful to adjust data previously processed without γ correction. Alternately, γ correction can be applied directly when FRET is calculated from the donor and acceptor intensity as described in the text.

Ensemble Fluorimetry

Ensemble fluorescence measurements were made on an SLM AMINCO-Bowman Series 2 spectrofluorimeter (Thermo Fisher Scientific, Waltham, MA). Quantum yield (φ) measurements were made relative to Rhodamine 101 in ethanol and Cresyl Violet in methanol (Sigma-Aldrich, St. Louis, MO). Quantum yield measurements were made by adjusting

unknown and reference samples to the same absorbance value (A.U. = 0.5) at the peak wavelength of excitation. The unknown and reference samples were then measured at several concentrations using identical series dilution. By cross checking different φ standards (Cresyl Violet in methanol and Rhodamine 101 ethanol), we found that determining φ relative to standards was most effective when measured at several concentrations by series dilution rather than a single point (data not shown). Avoiding normalization by low absorbance values also improved repeatability.

Empirical Determination of Instrument Factor ($\eta_{A/D}$)

Singly-labeled DNA samples were generated by annealing to unlabeled strands. For single color measurements on doubly-labeled constructs we utilized selective photobleaching to destroy the other dye prior to measurement. Following immobilization, the same samples were measured under both optical paths 1 and 3. A 532 nm laser at varying powers was used to stimulate both donor and acceptor molecules, with the laser power being measured immediately before the quartz prism. Individual molecules were identified by single step photobleaching events and the average intensity prior to photobleaching was calculated. The mean intensity for all molecules within the field of view was repeatedly measured to reduce error arising from inhomogeneous illumination. A linear fit of results for at least four different laser powers was applied to both donor and acceptor emission. The slopes of laser power dependence of single molecule emission intensity were normalized by ensemble measurements that determined the sample-concentration dependence of the total emission intensity. Total emission intensity was determined by collecting the complete spectrum, applying spectral calibration factors supplied by the manufacturer to account for the instrument response, and integrating the area under the resultant curve. Ensemble experiments were measured with excitation at 532 nm.

This procedure was repeated with a protein sample of PSD-95 that was singly-labeled at A230C with either Alexa 555 or Alexa 647. After encapsulation in egg phosphatidylcholine liposomes, the same donor samples (Alexa 555) were excited at 532 nm and the acceptor samples (Alexa 647) were excited at 633 nm. The focus of each laser was adjusted to ensure that all excited molecules occurred within the field of view. As with DNA, the slopes of laser illumination power dependence of single molecule fluorescence emission were normalized by the slope of ensemble concentration dependence. In this case, separate excitation wavelengths

were used (532 nm for donor and 633 nm for acceptor) to match the conditions single-molecule experiment.

Protein Constructs

The native cysteines in PSD-95 were mutated to serines to allow for the introduction of unique labeling sites. Using the high resolution NMR structure of N-terminal PDZ domains of PSD-95 (3), we chose labeling sites that place the introduced cysteine residue at a surface-exposed location with a minimum of possible near neighbor interactions, intramolecular hydrogen bonds or salt bridges. For empirical $\eta_{A/D}$ measurements, we used a sample with a mutation (A230C) that places the label in a surface exposed position in the second PDZ domain (3). The two samples FRET samples had a second labeling site positioned at one of two surface exposed locations in the first PDZ domain (E135C (PSD20) or S142C (PSD21)) that are 7 residues apart in the primary sequence. Protein was purified using Ni-NTA beads (QIAGEN, Valencia, CA) and a monoQ column (GE Healthcare, Piscataway, NJ). Purified PSD-95 is monodisperse, elutes as a single peak from size exclusion chromatography, gives a single peak of the expected MW on MALDI mass spectrometry, and binds physiologically-relevant peptide ligands (data not shown). Labeling the protein does not change the behavior on size exclusion chromatography indicating a lack of gross structural changes. Anisotropy of conjugated dyes is similar to that of the free dye. The protein remains completely soluble indicating no aggregation. Labeled protein also interacts with physiological ligands and displays appropriate physiological specificity. By these measures PSD-95 tolerates the labels well (data not shown). The protein FRET samples were randomly labeled with a mixture of Alexa donor and acceptor fluorophores with 1:1 stoichiometry to greater than 90% efficiency resulting in a mixed population (DD, 2DA, AA). The two DA species were indistinguishable in the analysis and were assumed to be identical with respect to their FRET efficiency. After labeling, samples were desalted on Sephadex G-50 and further purified by gel filtration on Superdex S200 (GE Healthcare, Piscataway, NJ). For liposome encapsulation by extrusion the protein was mixed at 1 μM with 20 mg/mL egg phosphotidylcholine containing 0.5 mol % of biotin- phosphatidylethanolamine (Avanti Polar Lipids, Alabaster, AL). Free protein was removed by gel filtration on CL-4B resin (GE Healthcare, Piscataway, NJ).

Supporting References

1. Bowen, M. E., K. Weninger, J. Ernst, S. Chu, and A. T. Brunger. 2005. Single-molecule studies of synaptotagmin and complexin binding to the SNARE complex. Biophys J 89:690-702.
2. Weninger, K., M. E. Bowen, U. B. Choi, S. Chu, and A. T. Brunger. 2008. Accessory proteins stabilize the acceptor complex for synaptobrevin, the 1:1 syntaxin/SNAP-25 complex. Structure 16:308-320.
3. Long, J.-F., H. Tochio, P. Wang, J.-S. Fan, C. Sala, M. Niethammer, M. Sheng, and M. Zhang. 2003. Supramodular structure and synergistic target binding of the N-terminal tandem PDZ domains of PSD-95. Journal of Molecular Biology 327:203-214.

	Optical Path 1		Optical Path 2		Optical Path 3		
	Mean	**Width**	**Mean**	**Width**	**Mean**	**Width**	**Std Dev.**
DNA7	0.993	0.011	0.933	0.1034	0.947	0.059	0.0311
DNA10	0.800	0.115	0.624	0.1026	0.636	0.071	0.0983
DNA14	0.520	0.138	0.316	0.0592	0.279	0.054	0.1301
DNA19	0.136	0.068	0.092	0.0689	0.079	0.034	0.0298

Table S1. Raw Relative Proximity Ratios and Peak Widths for DNA Samples.

	Optical Path 1		Optical Path 2		Optical Path 3		
	Mean	**Width**	**Mean**	**Width**	**Mean**	**Width**	**Std Dev.**
DNA7	0.981	0.031	0.948	0.0812	0.943	0.062	0.0204
DNA10	0.738	0.139	0.679	0.0977	0.616	0.070	0.0609
DNA14	0.434	0.139	0.372	0.0689	0.265	0.049	0.0855
DNA19	0.100	0.052	0.116	0.0772	0.074	0.042	0.0212

Table S2. Corrected Relative Proximity Ratios and Peak Widths for DNA Samples Using $\eta_{A/D}$ from Optical Path Transmission and Detection.

	Optical path 1		Optical Path 2		Optical Path 3		
	Mean	**Width**	**Mean**	**Width**	**Mean**	**Width**	**Std Dev.**
DNA7	0.989	0.024	N/D	N/D	0.973	0.030	0.0111
DNA10	0.835	0.096	N/D	N/D	0.793	0.053	0.0299
DNA14	0.580	0.139	N/D	N/D	0.459	0.069	0.0859
DNA19	0.166	0.079	N/D	N/D	0.154	0.077	0.0089

Table S3. Corrected Relative Proximity Ratios and Peak Widths for DNA Samples Using $\eta_{A/D}$ from Empirical Measurements.

Sample	Ensemble QY		
	Donor	Acceptor	$\varphi_{A/D}$
Acceptor Strand	---	0.56	---
DNA7	0.33	---	1.70
DNA10	0.33	---	1.70
DNA14	0.32	---	1.75
DNA19	0.33	---	1.70
E135C	0.20	0.65	3.25
S142C	0.14	0.65	4.64
Y236C	0.23	0.63	2.74
S142C- Y236C	0.185 (mean)	0.64 (mean)	3.46
E135C- Y236C	0.215 (mean)	0.64 (mean)	2.98

Table S4. Ensemble Quantum Yields of DNA and Protein Samples Used in this Study.

	$\gamma^{Empirical}$		$\gamma^{Photobleach}$		
	Optical Path 1	Optical Path 3	Optical Path 1	Optical Path 2	Optical Path 3
DNA7	1.365	0.795	1.306	0.631	0.770
DNA10	1.350	0.786	1.262	0.758	0.647
DNA14	1.391	0.810	1.069	0.668	0.339
DNA19	1.332	0.775	0.794	0.515	0.393
S142C-Y236C	2.743	1.597	3.103	N/D	1.798
S135C-Y236C	2.378	1.385	2.237	N/D	1.083

Table S5. Comparison of $\gamma^{Empirical}$ and Global $\gamma^{Photobleach}$ for DNA and Protein Samples.

	Optical Path 1		Optical Path 2		Optical Path 3		
	Mean	Width	Mean	Width	Mean	Width	Std Dev.
DNA7	0.981	0.031	N/D	N/D	0.957	0.049	0.0170
DNA10	0.747	0.137	N/D	N/D	0.690	0.066	0.0406
DNA14	0.437	0.140	N/D	N/D	0.321	0.058	0.0816
DNA19	0.106	0.059	N/D	N/D	0.098	0.053	0.0054

Table S6. Corrected FRET Values and Peak Widths for DNA Samples Using $\gamma^{Empirical}$.

	Optical Path 1		Optical Path 2		Optical Path 3		
	Mean	Width	Mean	Width	Mean	Width	Std. Dev
Universal Normalization							
DNA7	0.984	0.029	0.958	0.066	0.968	0.036	0.0134
DNA10	0.776	0.124	0.726	0.775	0.755	0.059	0.0250
DNA14	0.483	0.141	0.424	0.406	0.406	0.067	0.0406
DNA19	0.120	0.061	0.138	0.128	0.128	0.064	0.0091
Global Normalization							
DNA7	0.981	0.030	0.950	0.078	0.958	0.047	0.0165
DNA10	0.759	0.134	0.716	0.086	0.730	0.059	0.0218
DNA14	0.503	0.142	0.476	0.075	0.493	0.064	0.0137
DNA19	0.165	0.079	0.216	0.139	0.176	0.084	0.0272
Individual Normalization							
DNA7	0.952	0.027	0.951	0.076	0.957	0.040	0.0032
DNA10	0.736	0.051	0.713	0.050	0.730	0.036	0.0121
DNA14	0.493	0.053	0.479	0.074	0.495	0.043	0.0084
DNA19	0.157	0.078	0.174	0.085	0.169	0.072	0.0089

Table S7. Effect of Varying the Application of $\gamma^{Photobleaching}$ on the Corrected FRET Values and Peak Widths for DNA Samples.

PSD20 (PSD-95 S142C - Y236C)					
Method	**Optical Path 1**		**Optical Path 3**		
	Mean	**Width**	**Mean**	**Width**	**Std. Dev**
Raw	0.675	0.125	0.554	0.163	0.0855
Empirical	0.425	0.126	0.440	0.164	0.0106
Global	0.389	0.119	0.410	0.160	0.0148
Individual	0.397	0.115	0.402	0.103	0.0035

PSD21 (PSD-95 E135C - Y236C)					
Method	**Optical Path 1**		**Optical Path 3**		
	Mean	**Width**	**Mean**	**Width**	**Std. Dev**
Raw	0.577	0.132	0.374	0.105	0.1448
Empirical	0.363	0.121	0.304	0.092	0.0417
Global	0.377	0.129	0.361	0.101	0.0113
Individual	0.367	0.109	0.356	0.096	0.0078

Table S8. Effect of Varying Methods of γ Normalization on the FRET Values and Peak Widths for Protein Samples.

Sample	Optical Path 1	Optical Path 2	Optical Path 3
DNA7	307	252	335
DNA10	175	98	344
DNA14	296	134	186
DNA19	122	65	297
S142C-Y236C	227	N/D	143
S135C-Y236C	203	N/D	167

Table S9. Number of Molecules for Each Sample Used in this Study.

Supporting Figure Legends

Figure S1. Empirical Determination of $\eta_{A/D}$

The single-molecule intensities for donor and acceptor dyes were measured at varying laser powers under differing optical paths. Both $\varphi_{A/D}$ and $\eta_{A/D}$ contribute to differences in the relative slopes between donor and acceptor dyes. Normalizing these values by ensemble measurements of the concentration-dependent emission of the same samples allows for the determination of $\eta_{A/D}$ for a given filter set. **(A)** DNA single-labeled with either Cy3 (green) or Cy5 (red) was excited at 532 nm. (Top) The average single-molecule intensities for these samples at different laser powers were measured under optical path 1 (——) and optical path 3 (-----). (Bottom) Ensemble fluorescence was measured at varying concentrations. $\eta_{A/D}$ was found to be 0.79 for optical path 1 and 0.46 for optical path 3. **(B)** PSD-95 was singly-labeled with either Alexa 555 (green) or Alexa 647 (red) and encapsulated in lipid vesicles. Different wavelengths were used for excitation: 532 nm for donor and 633 for acceptor. (Top) The average single-molecule intensities for these samples were measured under optical path 1 (——) and optical path 3 (-----) at varying laser powers. (Bottom) Ensemble fluorescence was measured at varying concentrations. Using these slopes, $\eta_{A/D}$ was found to be 0.77 for optical path 1 and 0.44 for optical path 3.

Figure S2. Single-Molecule Intensities of DNA Constructs

The average fluorescent intensity for each fluorescent dye on DNA7 (Orange), DNA10 (green), DNA14 (Purple) and DNA19 (blue) were individually measured at the single-molecule level. For 50 seconds stimulation by a 633 nm laser was used to excite Cy5, at which point all molecules within the field of view had been bleached. Following this, unbleached Cy3 was stimulated by a 532 nm laser for an equal period of time. The average intensities of all acceptable molecules, displaying single photobleaching events, were compiled into histograms. Both **(A)** Cy3 and **(B)** Cy5 intensities showed little variability between DNA samples, consistent with ensemble measurements.

Figure S3. Application of γ Normalization to Protein Samples and Comparison of γ Normalization Methods

Energy transfer for two PSD-95 mutant was measured under optical path 3. **(A)** Histogram of E_{PR} for PSD20 (*white*) and PSD21 (*gray*). Data points are shown as filled circles with the Gaussian fit shown as a solid line. **(B)** Histogram of γ values compiled from individual photobleaching events. **(C)** Histograms of normalized FRET efficiency calculated using $\gamma^{Individual}$. Because of differences in γ, samples with similar FRET display differing E_{PR}. **(D)** The standard deviation in the corrected mean FRET efficiency of each protein sample measured under the two different optical paths after the indicated method of γ normalization. Reduced standard deviation indicates convergence of the mean FRET efficiency after γ normalization is applied **(E)** The mean peak width for each protein sample under two optical paths. A reduced mean width

indicates narrower peaks after γ normalization. Error bars indicate the standard deviation between the mean widths measured under different filter sets after the indicated method of γ normalization. Unlike DNA, protein samples did not show a statistically significant reduction upon $\gamma^{Individual}$ normalization.

Figure S4. Distribution of γ within the FRET Peak for Proteins

The mean γ value for all molecules within each bin of the histograms for the raw relative proximity ratio (left) and after $\gamma^{Individual}$ normalization (right). **(A)** PSD20 and **(B)** PSD21 were measured under optical path 1. The value of mean γ for each bin of the FRET histogram is colored according to the scale bar shown beneath the panels. Because of differences in $\varphi_{A/D}$, different scales for γ were required to properly illustrate γ distributions. An increasing relative proximity ratio correlated with increased γ for uncorrected measurements. γ values are more evenly distributed in the $\gamma^{Individual}$ normalized FRET histogram but γ outliers still show outlying FRET values.

A

Cy Dyes on DNA
(532 nm Excitation)

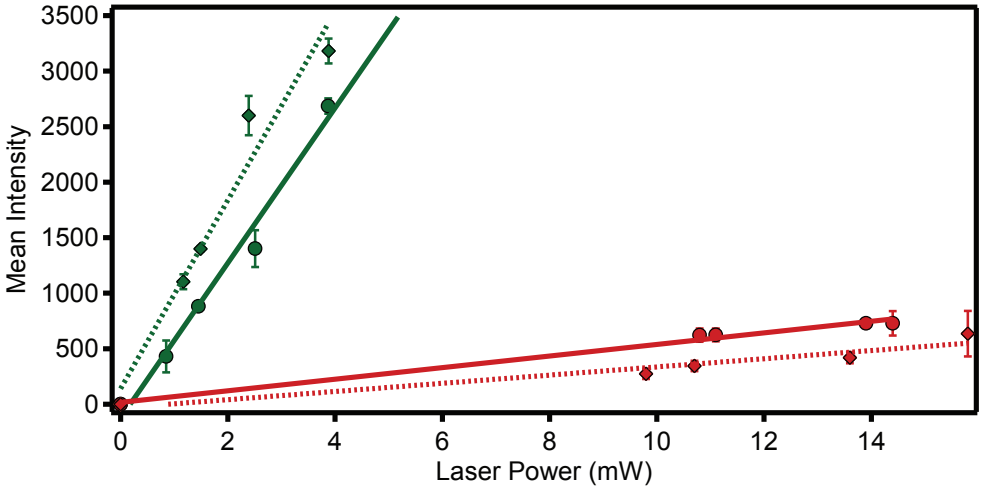

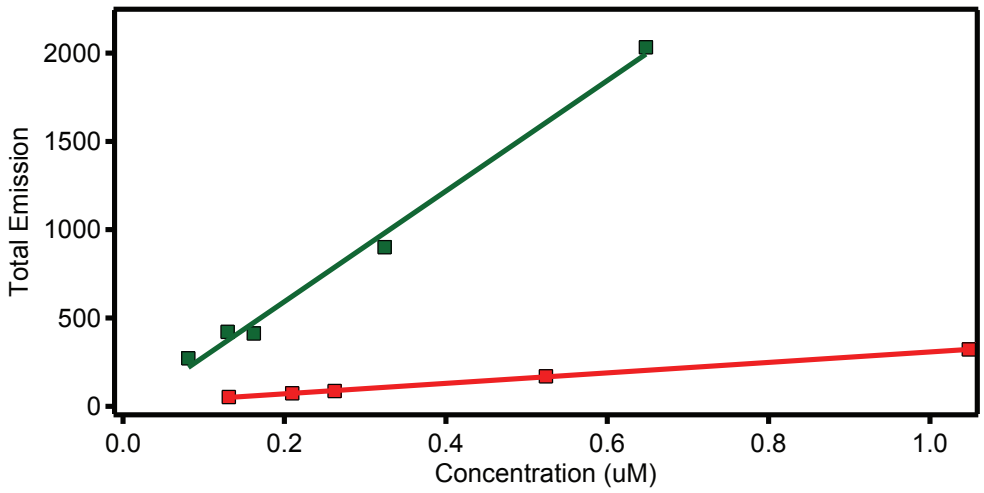

B

Alexa Dyes on Protein
(Separate Excitation)

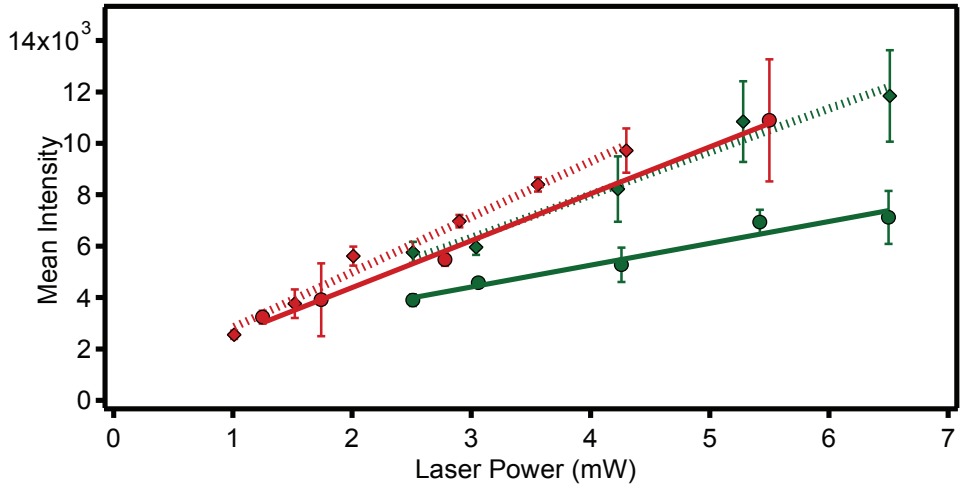

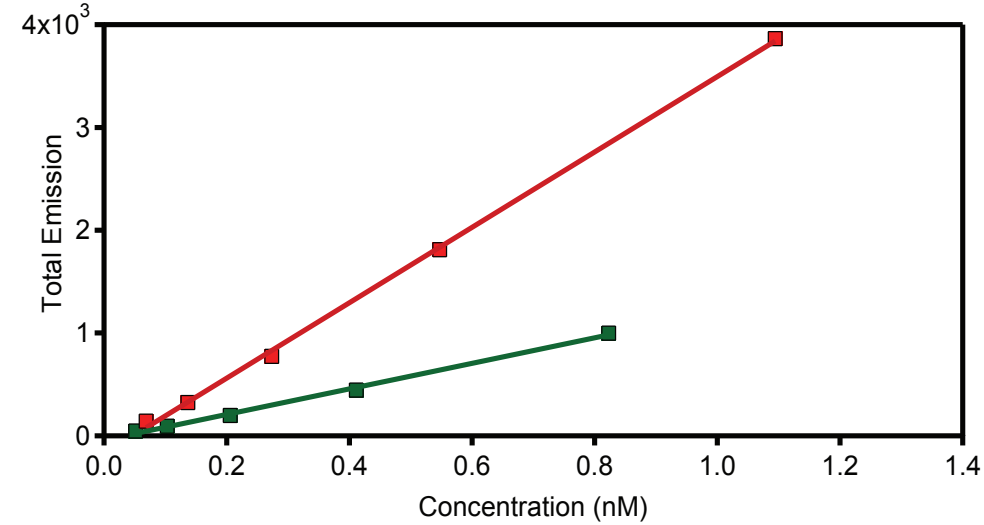

Supporting Figure 1

A

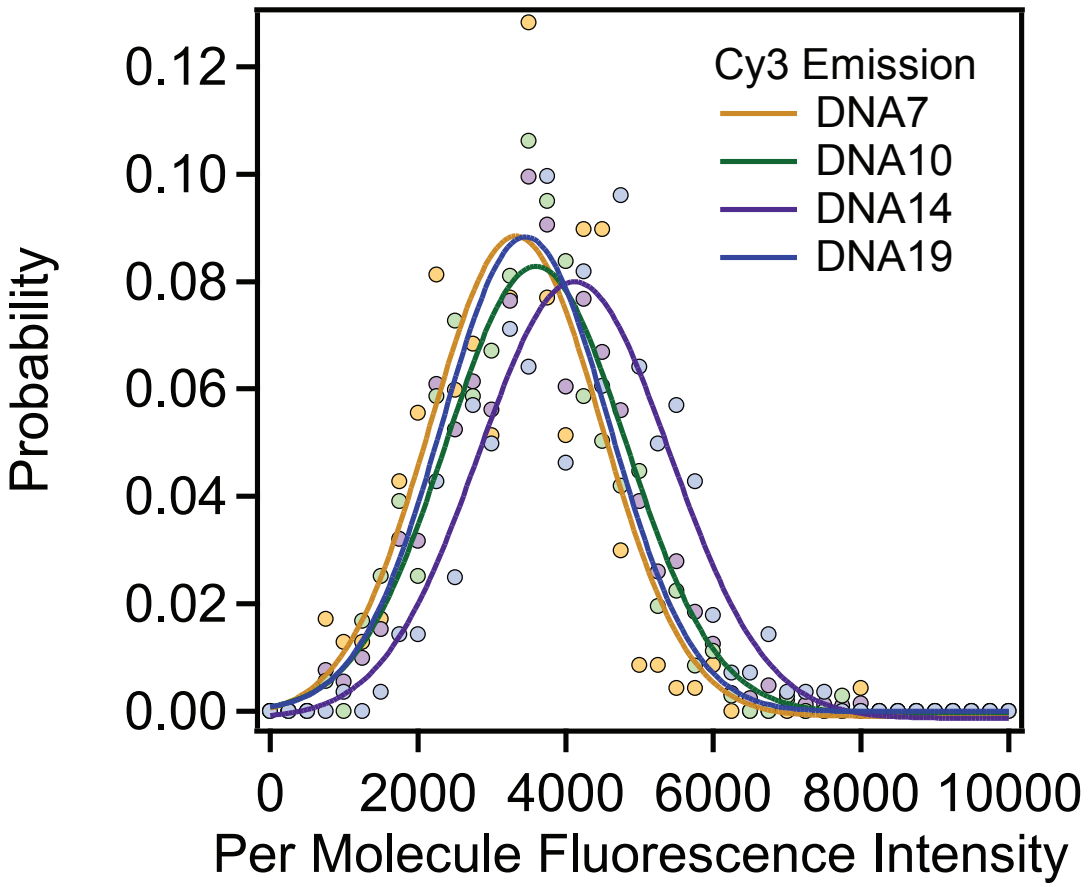

B

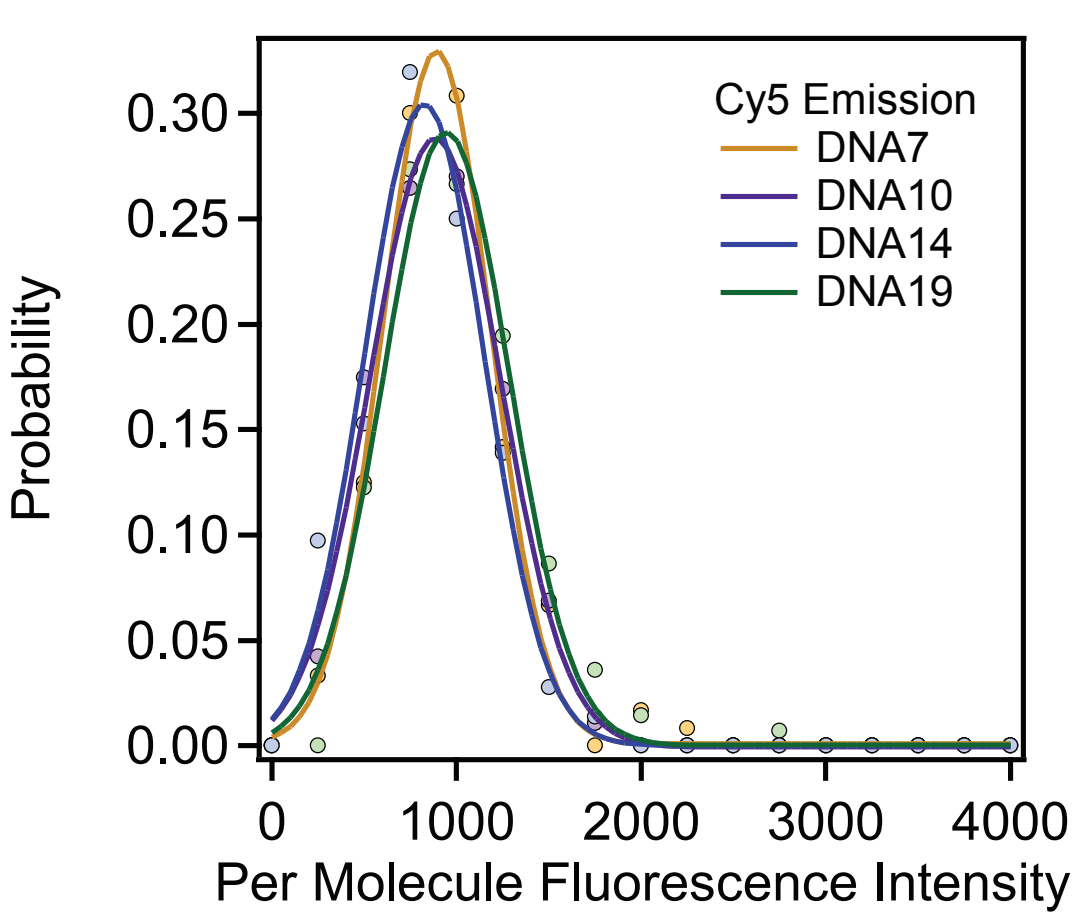

Supporting Figure 2

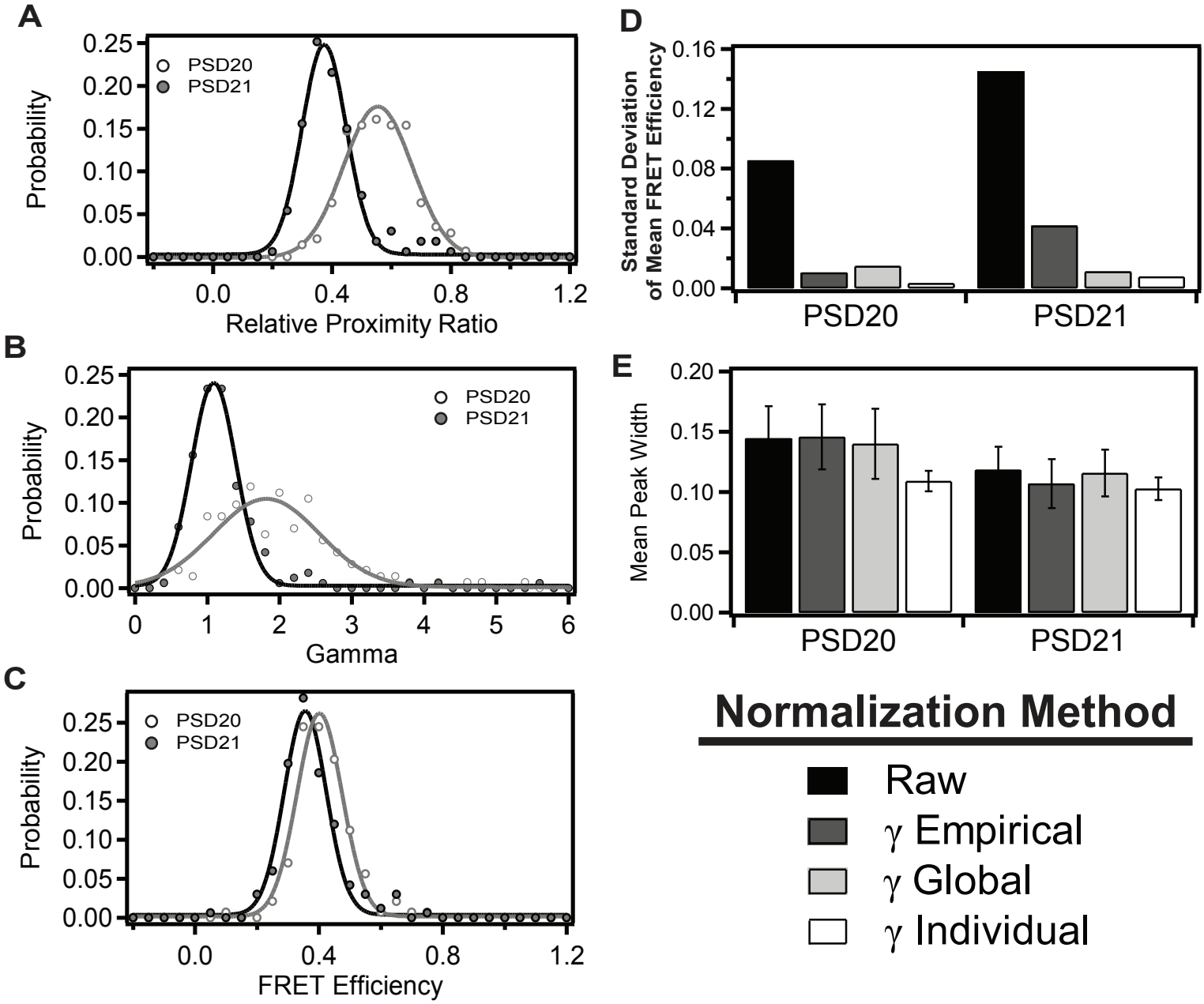

Supporting Figure 3

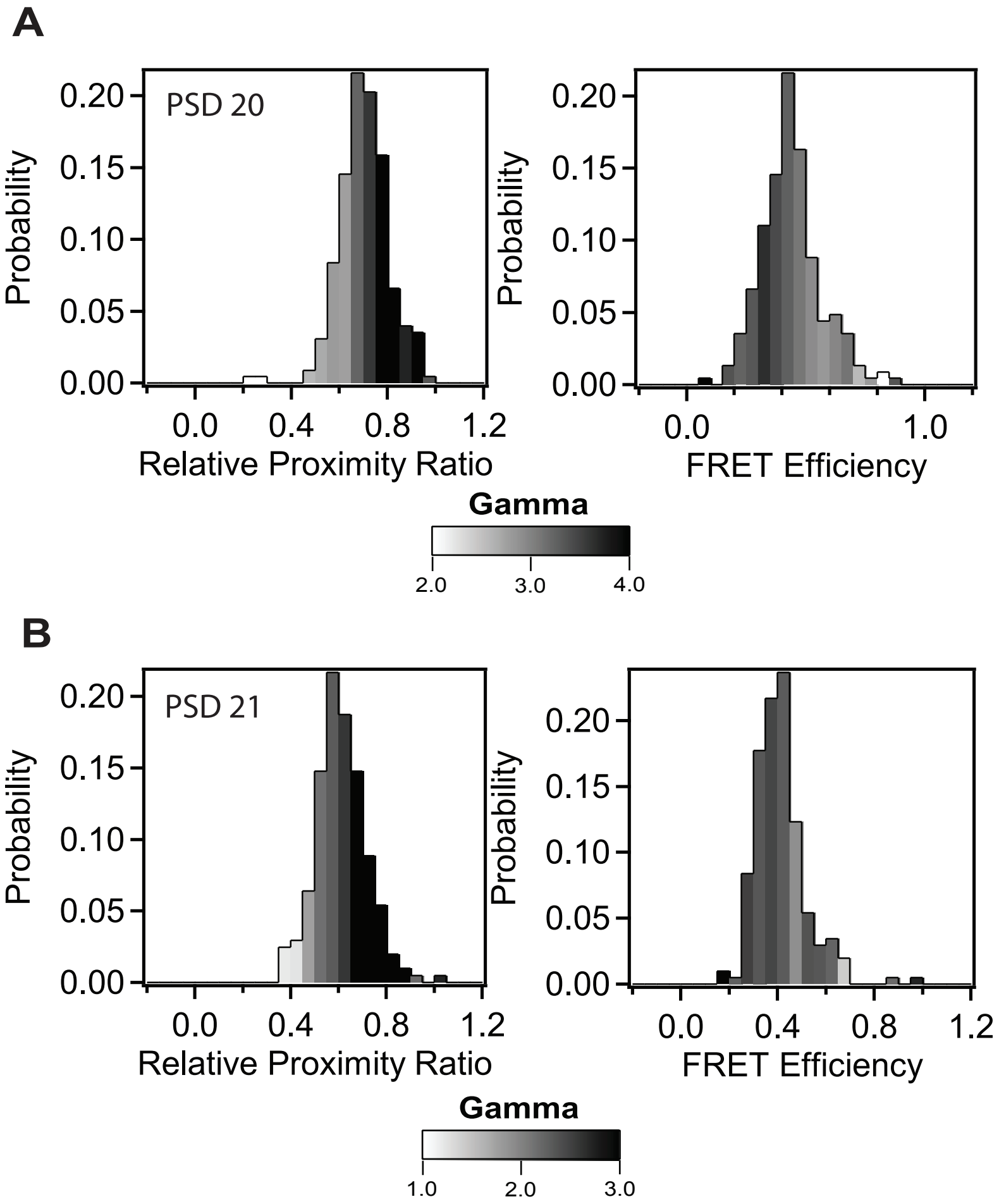

Supporting Figure 4